HAL
open science

Realization of Polaritonic Topological Charge at Room Temperature Using Polariton Bound States in the Continuum from Perovskite Metasurface

Nguyen Ha My Dang, Simone Zanotti, Emmanuel Drouard, Céline Chevalier, Hai Son Nguyen, Gaëlle Trippé-Allard, Mohamed Amara, Emmanuelle Deleporte, Vincenzo Ardizzone, Daniele Sanvitto, et al.

To cite this version:

Nguyen Ha My Dang, Simone Zanotti, Emmanuel Drouard, Céline Chevalier, Hai Son Nguyen, et al.. Realization of Polaritonic Topological Charge at Room Temperature Using Polariton Bound States in the Continuum from Perovskite Metasurface. Advanced Optical Materials, 2022, 10 (6), pp.2270021. 10.1002/adom.202102386 . hal-03708296

HAL Id: hal-03708296

https://hal.science/hal-03708296v1

Submitted on 12 Dec 2022

HAL is a multi-disciplinary open access archive for the deposit and dissemination of scientific research documents, whether they are published or not. The documents may come from teaching and research institutions in France or abroad, or from public or private research centers.

L'archive ouverte pluridisciplinaire **HAL**, est destinée au dépôt et à la diffusion de documents scientifiques de niveau recherche, publiés ou non, émanant des établissements d'enseignement et de recherche français ou étrangers, des laboratoires publics ou privés.

Realization of polaritonic topological charge at room temperature using polariton bound states in the continuum from perovskite metasurface

Nguyen Ha My Dang, *Simone Zanotti*, *Emmanuel Drouard*, *Céline Chevalier*, *Gaëlle Trippé-Allard*, *Mohamed Amara*, *Emmanuelle Deleporte*, *Vincenzo Ardizzone*, *Daniele Sanvitto*, *Lucio Claudio Andreani*, *Christian Seassal*, *Dario Gerace* and *Hai Son Nguyen**

N. H. M. Dang, Prof. E. Drouard, Dr. C. Chevalier, Dr. M. Amara, Dr. C. Seassal
Univ Lyon, Ecole Centrale de Lyon, CNRS, INSA Lyon, Université Claude Bernard Lyon 1, CPE Lyon, CNRS, INL, UMR5270, 69130 Ecully, France
S. Zanotti, Prof. L. C. Andreani, Prof. D. Gerace
Dipartimento di Fisica, Università di Pavia, via Bassi 6, I-27100 Pavia, Italy
Dr. G. Trippé-Allard, Prof. E. Deleporte
Université Paris-Saclay, ENS Paris-Saclay, CNRS, CentraleSupélec, LuMIn, Gif-sur-Yvette, France
Dr. V. Ardizzone, Dr. D. Sanvitto
CNR Nanotec, Institute of Nanotechnology, via Monteroni, 73100, Lecce, Italy
Prof. H. S. Nguyen
Univ Lyon, Ecole Centrale de Lyon, CNRS, INSA Lyon, Université Claude Bernard Lyon 1, CPE Lyon, CNRS, INL, UMR5270, 69130 Ecully, France
IUF, Université de France
Email Address: hai-son.nguyen@ec-lyon.fr

Keywords: *exciton-polaritons, strong coupling regime, hybrid perovskite, bound states in the continuum, polarization vortex, topological charge, resonant metasurface*

Exciton-polaritons are mixed light-matter excitations resulting from the strong coupling regime between an active excitonic material and photonic resonances. Harnessing these hybrid excitations provides a rich playground to explore fascinating fundamental features, as out-of-equilibrium Bose-Einstein condensation and quantum fluids of light, plus novel mechanisms to be exploited in optoelectronic devices. We investigate experimentally the formation of exciton-polaritons arising from the mixing between hybrid inorganic-organic perovskite excitons and an optical Bound state In a Continuum (BIC) of a subwavelength-scale metasurface, at room temperature. These polaritonic eigenmodes, hereby called polariton BICs (pol-BICs) are revealed in reflectivity, resonant scattering, and photoluminescence measurements. Although pol-BICs only exhibit a finite quality factor bounded by the non-radiative losses of the excitonic component, they fully inherit BIC peculiar features: a full uncoupling from the radiative continuum in the vertical direction, which is associated to a locally vanishing farfield radiation in momentum space. Most importantly, our experimental results confirm that the topological nature of the photonic BIC is perfectly transferred to the pol-BIC. This is evidenced by the observation of a polarization vortex in the farfield of polaritonic emission. Our results pave the way to engineer BIC physics of interacting bosons and novel room temperature polaritonic devices.

1 Introduction

Bound states in the Continuum (BICs) are peculiar localized states that are forbidden to radiate despite lying in a continuum of propagating waves. Once regarded as an 'exotic' quantum mechanical effect,[1] the origin of BICs is nowadays fully unraveled as a particular solution of wave equations, which has led to their exploitation in other fields where it is straightforwardly attributed to destructive interference mechanisms or symmetry mismatches.[2] The most active playground of BIC physics is in contemporary Photonics[3] since most of optoelectronic devices rely on resonances and their coupling mechanisms with environment. Indeed, the trapping of light through photonic BICs is a salient feature to enhance different light-matter interaction mechanisms, leading to various applications in microlasers,[4, 5, 6, 7, 8] sensors,[9] optical switches[7] and nonlinear optics.[10, 11, 12, 13] Moreover, on the fundamental side, photonic BICs in periodic lattices are pinned to singularities of farfield polarization vortex and can be considered as topological charges of non-Hermitian systems.[14, 15, 16, 17] This topological nature, together with modern technological feasibility to tailor photonic materials, makes photonic BICs a fruitful platform to engineer polarization singularities of open photonic systems.[18, 5, 19, 20]

Another prominent area of investigation in modern Optics is represented by exciton-polaritons, elementary excitations arising from the strong coupling regime between confined light and semiconductor excitons.[21] As hybridized eigenmodes, these bosonic quasiparticles inherit original features of both photonic resonances and excitonic ones. During the last decades, exciton-polaritons have become a standard platform to explore exotic phenomena of out-of-equilibrium Bose-Einstein condensations[22] and quantum fluid properties of electromagnetic fields,[23] as well as novel concepts for all-optical devices. While most of the milestones of polaritonic physics have been achieved with excitonic materials operating at cryogenic temperatures ($\sim 10\,\mathrm{K}$), recent progress in materials science has promoted many polaritonic demonstrations at room temperature with a wide variety of high bandgap semiconductors, ranging from GaN,[24, 25] ZnO,[26] to organic semiconductors[27, 28] and transition metal dichalcogenide monolayers,[29, 30] as well as perovskite materials.[31, 32, 33, 34, 35, 36, 37, 38, 39, 40, 41]

Very recently, the strong coupling regime between photonic BICs and excitonic resonances has been theoretically suggested,[42, 43, 44, 45] with two experimental demonstrations.[46, 47] The result of such a coupling is the formation of polariton-BICs (pol-BICs): hybrid excitations that are completely decoupled from the radiative continuum. This scenario is quite different from the text-book architecture in which the strong coupling regime is engineered by embedding quantum wells at the antinode positions of planar microcavities, which always exhibit substantial nonradiative losses. As state-of-the-art, non-linear behaviors of pol-BICs[46] and the use of pol-BICs to trigger Bose-Einstein Condensation have been recently demonstrated.[47] However, most of these demonstrations are conducted at cryogenic temperatures. Therefore, making pol-BICs with room temperature operation would be the next important step for the development of polaritonic devices based on BIC concepts.

Perovskite materials have appeared in the last few years as the ideal alternative candidate to study exciton-polaritons at room temperature.[48] Nowadays, polaritonic Bose-Einstein condensation in the perovskite platform can be engineered to reproduce many features that have been up to now only evidenced in cryogenic GaAs-based polaritons.[34, 35, 37, 38] Moreover, the possibility to obtain high quality perovskite layers via solution-based methods opens feasible and low-cost approaches to fabricate perovskite metasurfaces. In this approach, the tailoring of the real part (i.e. frequency) of polaritonic energy-momentum dispersion has been experimentally demonstrated with sub-wavelength perovskite metasurface, in which linear, parabolic, and multi-valley dispersion characteristics have been reported.[38] Most recently, it has been theoretically suggested that perovskite metasurfaces can be harnessed to engineer the imaginary part (i.e., losses) of the polaritonic energy-momentum dispersion at room temperature via BIC and Exceptional Point concepts.[43, 45] On the other hand, purely photonic BICs in perovskite-based resonant metasurface have been reported to make ultra-fast switches[7] and tunable microlasers.[49]

In this work, we experimentally demonstrate the formation of pol-BICs in an excitonic metasurface made from hybrid 2D perovskites. The pol-BICs, revealed in reflectivity, resonant scattering, and photoluminescence measurements, are robust at room temperature. They are originated from the strong coupling regime between a symmetry-protected BIC and the excitonic resonance of the perovskite material. Although the pol-BICs only exhibit finite quality factor, which is actually limited by the non-radiative losses arising from the excitonic component, they fully inherit the purely photonic BIC peculiar features: the decoupling from the radiative continuum, and the farfield emission vanishing at Γ point. Remarkably, the pol-BICs also inherit the topological nature of the purely photonic BICs. This is demonstrated through the observation of a polarization vortex in the farfield emission of pol-BIC modes.

2 Results and Discussion

2.1 Strong coupling between photonic BIC and excitonic resonance

Our excitonic material is a 2D layered hybrid organic-inorganic perovskite, namely bi-(phenethylammonium) tetraiodoplumbate, known as PEPI, with chemical formula $(C_6H_5C_2H_4NH_3)_2PbI_4$. Thanks to the alternation between organic and inorganic monolayers (see Figure 1c), PEPI thin films behave like a multi-quantum well structure where excitons are confined within inorganic monolayers. PEPI is one of the most widespread perovskite materials for polaritonic applications, thanks to its giant exciton binding energy (~ hundred meV at room temperature).[50] Here the fabrication of PEPI metasurface follows the same method previously reported (see Figure 1 for a simplified sketch).[38] The PEPI solution is infiltrated inside air holes of a pre-patterned silica backbone via spincoating, then followed by thermal annealing to form a square lattice of crystallized PEPI nano-pillars. The final sample is encapsulated with Poly-methyl methacrylate (PMMA) to protect PEPI against humidity.

The metasurface is designed so that the exciton energy (E_X = 2.394 eV) is in the vicinity of the lowest

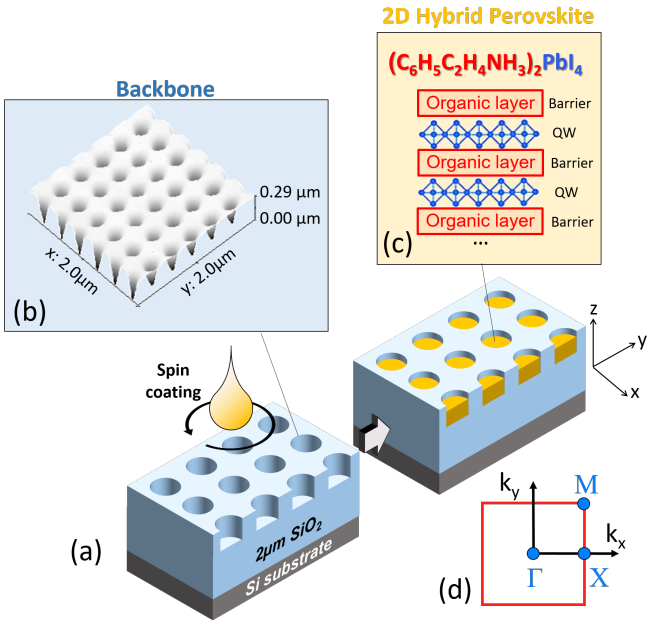

Figure 1: (a). Sketch of the fabrication method of the perovskite metasurface. The backbone consists of a 2 μm-thick thermal SiO_2 on silicon substrate. It is pre-patterned into a square lattice of holes, with period $a = 330$ nm, diameter $d = 132$ nm and depth $t_{SiO2} = 150$ nm. The crystallized perovskite layer has a total thickness $t_{PEPI} = 180$ nm. Thus there is a residual 30 nm-PEPI slab (not shown in the sketch). The final structure is encapsulated by 200 nm-thick PMMA (not shown in the sketch). (b) Atomic Force Microscopy (AFM) image of the photonic backbone. (c) The layered structure of PEPI. (d) The reciprocal space with Brillouin zone of size $2\pi/a$, corresponding to a square lattice of period a.

Bloch resonances of the passive structure (PEPI is replaced by a dielectric material of constant refractive index $n = 2.4$). In Figure 2a we report the energy-momentum dispersion and the corresponding quality factor (color-coded into the plot by points) of such Bloch resonances as calculated by Guided-Mode Expansion (GME) method,[51] generalized to deal with multilayered and partially etched dielectric materials.[52] The dispersion is calculated along ΓX direction (i.e. k_x, see Figure 1d). Only modes with an odd parity with respect to mirror symmetry for reflection through the xz ($y = 0$) plane are shown in Figure 2a (see Supporting Information for the whole spectrum including even modes), which can be excited by transverse-electric polarized incident radiation. These results show that the lowest mode is a bright (low Q-factor) one at Γ point, while two singly-degenerate BICs are present at slightly higher energy, here denoted BIC_1 and BIC_2. The theoretical electric field patterns of these two photonic BICs are reported in Figure 2b,c, showing both E_x and E_y components, both in vertical and planar cross sections. The odd parity of these spatial profiles for mirror symmetry through either xz or yz planes confirms that they are both symmetry-protected BICs, i.e., they are forbidden to couple to the radiative continuum due to their symmetry mismatch with radiative plane waves. As a result of numerical simulations using the Rigorous Coupled Wave Analysis (RCWA) method, Figure 2d presents the calculated angle-resolved reflectivity of the passive structure when excited by $\updownarrow$ (i.e. y) polarized light, that is s-polarized (transverse electric, TE) with respect to the xz plane of incidence. These results show very good agreement with the GME calculations for odd modes, we clearly distinguish the two BICs corresponding to the local vanishings of reflectivity resonances at $k_x = 0$. We also notice that only a singly degenerate leaky mode is shown in

Figure 2d with a maximum slightly below 2.3 eV, which matches the result in Figure 2a. The other mode, degenerates in Γ, is of ↔ (i.e., x) polarization (clearly evidenced in the corresponding GME results for even modes and the corresponding RCWA simulations for p-polarized (transverse magnetic, TM) excitation with respect to the xz incidence plane, shown in Supporting Information).

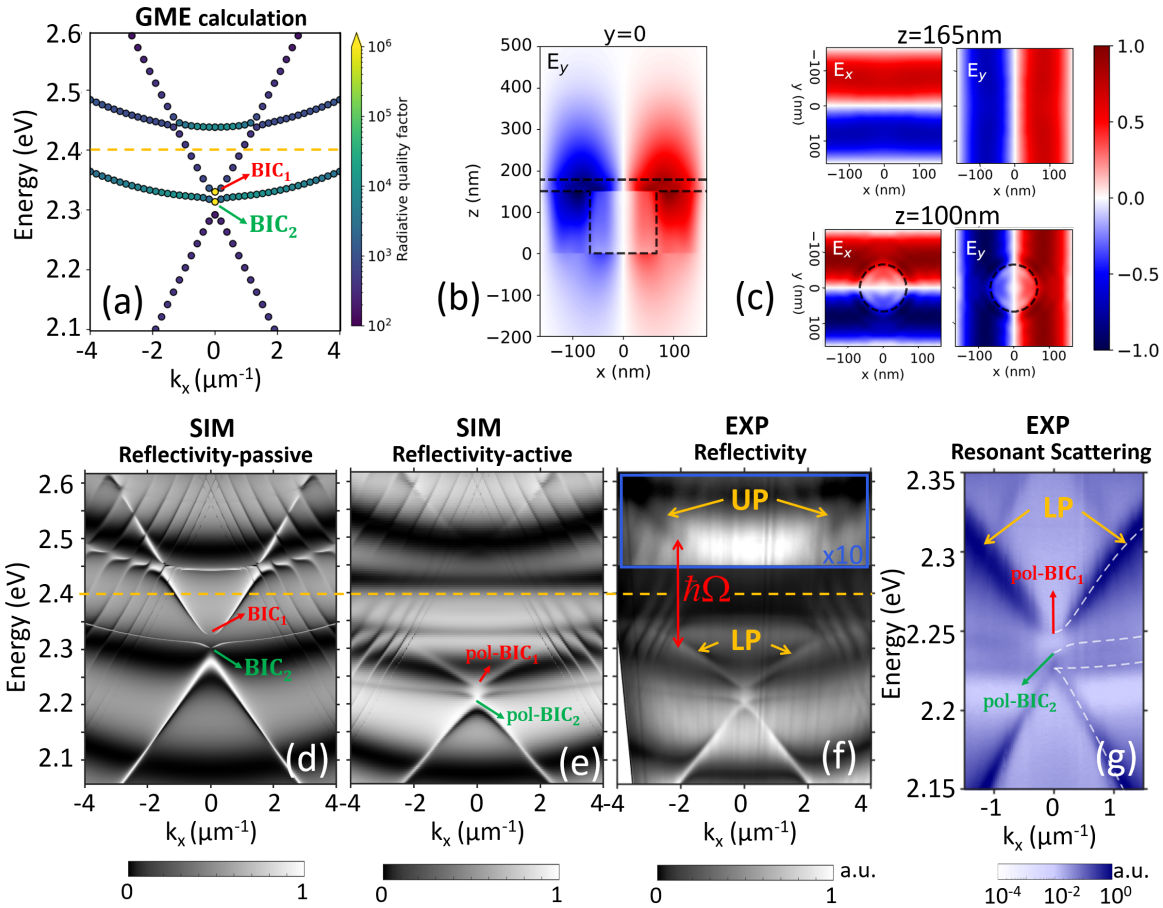

Figure 2: (a) Energy-momentum dispersion calculated by GME for the passive metasurface by GME method for odd modes with respect to mirror symmetry for reflection against the xz plane (at $y = 0$); the Q-factor of each k_x−dependent mode is encoded in the color scale of each point (yellow corresponds to virtually infinite Q-factor, as determined from GME simulations). The dotted orange line indicates the exciton energy: $E_X = 2.394$ eV, and it is shown here for illustration purposes. (b) Spatial distribution of the electric field in the xz plane within a single unit cell of the square lattice, as obtained for the BIC$_1$ mode, and (c) corresponding cross sections in the xy plane for two different vertical coordinates, corresponding either to the patterned region (PEPI infiltrated hole) or the uniform PEPI region; we notice that the calculated field distribution for the BIC$_2$ is very similar. (d) Numerical simulations of the angle-resolved reflectivity spectra calculated for the passive structure (assuming the same parameters as the GME calculation), and (e) same simulation for the active structure (i.e., assuming a Lorentz oscillator model for the PEPI material, see experimental section), when excited by ↕ (i.e. y) polarized light; also here the dashed line indicates the bare excitonic resonance of PEPI. (f) Experimental result of the angle-resolved reflectivity of the PEPI metasurface when excited by ↕ polarized light. The measured Rabi splitting is $\hbar\Omega \approx 200$ meV. (g) Experimental result of the angle-resolved resonant scattering of the PEPI metasurface, zoomed in the vicinity of the two pol-BICs. The excitation is polarized along ⤢ (i.e. 45 degrees) and the detection is analyzed along ⤡ (i.e. -45 degrees). The dotted lines are guides to the eye to distinguish the 4 polaritonic modes.

We now investigate the coupling -between PEPI excitons and the previous Bloch resonances, giving rise to

polaritonic modes[53]. A home-built setup for Fourier spectroscopy is employed to study the excitonic metasurface via angle-resolved and spectral-resolved experiments. The experimental results of angle-resolved reflectivity measurements (Figure 2f) and numerical ones from RCWA simulation (Figure 2e) are in perfect agreement. The strong coupling regime is evidently demonstrated in both experimental and numerical results, by comparison with the simulations of the passive structures (i.e., without considering the excitonic response) in Figure 2d. Indeed, all dispersion curves are strongly red-shifted from the bare exciton energy to form polaritonic branches. In particular, the anticrossings between the first lower polariton branch, here denoted LP, and the first upper polariton branch, here denoted UP, are clearly evidenced. The measured Rabi splitting is $\hbar\Omega \approx 200$ meV, which is in good agreement with previous reports on polaritons in PEPI metasurface,[38] as well as from the known expression for the radiation-matter coupling in confined systems in terms of the bulk material one,[54] see also details in experimental section.

Since the polaritonic modes inherit the symmetry properties of their photonic component, the first two LP branches possess the same odd parity at Γ point as the one of BIC_1 and BIC_2. Therefore, they must be symmetry-protected pol-BICs, denoted as pol-BIC_1 and pol-BIC_2, according to their photonic counterparts. To evidence their decoupling from the radiative electromagnetic continuum, a straightforward criterion is the vanishing of these resonances at Γ point, i.e. at normal incidence with respect to the metasurface. Although these vanishing resonances are hinted in Figures 2e,f, it is a tricky observation because the reflectivity resonances corresponding to these guided modes have Fano-like profiles superimposed on a shallow Fabry-Perot modulation deriving from the 2 μm-thick SiO_2.[55] We get rid of such a background by employing resonant scattering measurements,[56] in which the excitation and detection are in cross-polarization configuration (excitation in 45-degrees polarization direction, and analyzed in -45-degrees one). As shown in Figure 2g, we observe all four polariton lower branches, corresponding to the four Bloch resonances previously discussed. Notably, the resonant scattering results feature both E_x and E_y polarized modes. Indeed, the leaky branch of high curvature of E_x polarization is observed in resonant scattering results, and not in reflectivity measurements of E_y polarization. Most importantly, as expected, the resonant scattering vanishes locally at the two pol-BICs.

The reflectivity and resonant scattering measurements show that the PEPI metasurface can host pol-BICs modes. To populate these polaritonic modes and study their farfield emission, we perform non-resonant pumping (λ_{laser} = 400 nm, 80 MHz, 50 ps) with the same Fourier spectroscopy setup. Angle-resolved photoluminescence results, shown in Figure 3a, indicate that only the LP branch is efficiently populated while other modes (the UP and photonic-like bands at low energy) are either not observed or weakly populated. This observation is in good agreement with polaritonic behaviors in high bandgap materials for which the photoluminescence emission is mainly visible for the first lower polariton branch. The farfield emission of the LP vanishes locally at $k_x = 0$ where the pol-BIC_1 resides. Such effect, already shown in Figure 3a, is clearly evidenced in Figure 3b where the photoluminescence intensity of the LP is tracked and reported. We note that the excitonic fraction of the pol-BIC_1 amounts to 35% as estimated from

a simple model of two coupled oscillators, in which we take half of the Rabi splitting as the radiation-matter coupling energy (off-diagonal element in the 2 matrix, much larger than the oscillators linewidths) and the exciton-photon detuning estimated from the passive photonic BIC_1 mode (Figure 2a) indicating that it is indeed a hybrid exciton-photon entity.

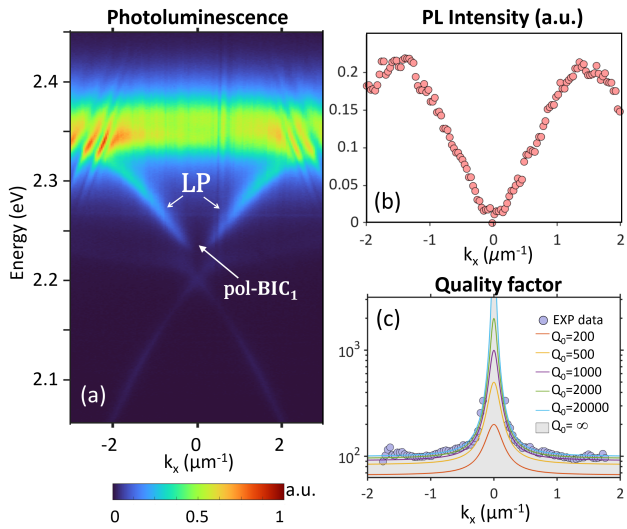

Figure 3: (a) Angle-resolved photoluminescence results, analysed along ↕(i.e. y). (b) Angle-resolved emission intensity of the LP. (c) The quality factor of the LP extracted from the photoluminescence measurements. The blue circles are experimental data, the solid lines correspond to the model (1) with $Q_\infty = 95$, $\alpha = 5.9\,\mu\text{m}^2$ but using different values of Q_0. The gray shading area corresponds to $Q_0 = \infty$.

2.2 Quality factor enhancement at pol-BICs

We now discuss on the use of photonic BICs to enhance the quality factor of polaritonic modes. Although this effect has been briefly mentioned in Ref[46], the underlying mechanism of quality factor enhancement, as well as its intrinsic limit has not been reported yet. Since photonic BICs possess an ideally infinite quality factor, one may expect the same for pol-BICs. However, due to their hybrid exciton-photon nature, the quality factor of pol-BICs is balanced between the non-radiative losses of the excitonic component and the one from the photonic BIC.[43] They are thus quasi-BICs, whose quality factor is limited by non-radiative losses. Moreover, the C_4 symmetry of the square-lattice imposes that the quality factor of photonic BICs decreases as k_x^2 at oblique angles.[5] Therefore, within a small angular window close to normal incidence, the quality factor $Q(k_x)$ of the LP can be determined from a relatively simple law:

$$Q(k_x)^{-1} = Q_0^{-1} + \left(Q_\infty + \frac{\alpha}{k_x^2}\right)^{-1}, \tag{1}$$

in which Q_0 corresponds to the non-radiative losses originated from the excitonic component, Q_∞ corresponds to the radiative losses of the photonic BIC at high oblique angles, and the coefficient α dictates the decreasing rate of the photonic BIC. Figure 3c depicts the angular dependence of the quality factor of the LPB extracted from the photoluminescence spectra. The value of Q_∞ is easily extracted from the experimental data. Indeed, assuming that $Q_\infty \ll Q_0$, the value of Q_∞ corresponds to the measured quality factor at high wavevector($> 1.5\,\mu\mathrm{m}^{-1}$). Thus $Q_\infty \approx 100$. The value of Q_0 is more tricky to obtain since the photoluminescence signal from normal emission angle is strictly zero due to the BIC nature. Nevertheless, we can use the angular dependence of the quality factor to evaluate Q_0. The experimental data are nicely fitted by the model (1), with $Q_\infty = 95$, $\alpha = 5.9\,\mu\mathrm{m}^2$ and Q_0>1000. Therefore, our pol-BIC exhibits a quasi-BIC nature, indeed, having infinite radiative quality factor inherited from the photonic component, but a finite non-radiative one (>1000) inherited from the excitonic component. This property is fundamental and crucial for designing polaritonic devices using BIC concepts: there is a trade-off between infinite quality factor (from photonic fraction) and giant nonlinearity (from excitonic fraction).

2.3 Topological nature of pol-BICs

Finally, we focus the discussion on the topological nature of pol-BICs. To our knowledge, this fundamental property of pol-BICs has not been addressed in the literature, so far, either theoretically or experimentally. Despite being quasi-BICs with finite quality factor, pol-BICs preserve the nature of singularities in momentum space. This is due to a complete decoupling from the radiative continuum. As a consequence, every polaritonic branch that hosts a pol-BIC mode exhibits a polarization vortex around this singularity. Thus, pol-BICs fully inherit the topological behavior of their photonic components.

We first verify the topological nature of the purely photonic BIC_1 of the passive photonic structure (see Figure 2a, and details in Supporting Information) calculated from the GME results. Figures 4a,b depict the theoretically determined Stokes parameters S_1 and S_2 of the photonic BIC_1. These results clearly evidence the existence of a polarization singularity at the Γ point in reciprocal space. From the mapping of S_1 and S_2, we can easily extract the polarization orientation, ϕ, given by the relation $\tan\{2\phi\} = S_2/S_1$. The latter is -reported in Figure 4c, showing that ϕ decreases by an angle 2π when the Γ point is encircled. Therefore, the photonic BIC_1 is associated to a topological charge q, given by:[14]

$$q = \frac{1}{2\pi} \oint_C dk.\nabla_k \phi = -1. \tag{2}$$

This numerical result is in good agreement with the topological charge predicted by group theory corresponding to the C_4 in-plane symmetry of our square lattice (see details in Supporting Information). We now investigate experimentally the polarization pattern of the LP branch in the vicinity of the pol-BIC_1. Figures 4a',b',c' present the measured Stokes parameters S_1 (Figure 4a'), S_2 (Figure 4b') and the extracted orientation ϕ (Figure 4c'). The corresponding numerical results of the active structure, obtained by RCWA simulations, are presented in Figures 4a",b",c", showing almost perfect agreement with the

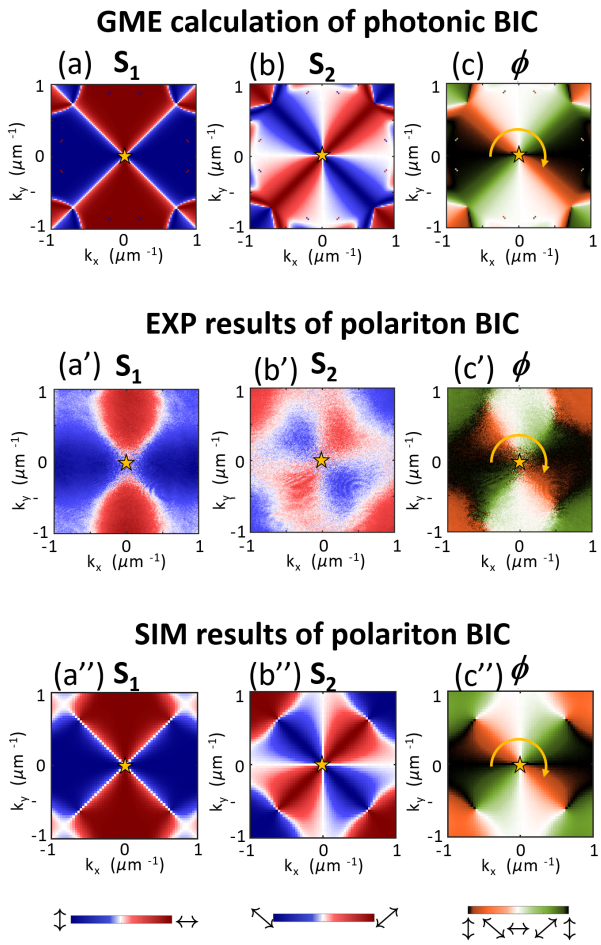

Figure 4: Theoretical Stokes parameters S_1 (a), S_2 (b), and the polarization orientation ϕ (c) as obtained from GME simulations of the passive structure and corresponding to the BIC$_1$ Bloch mode of Figure 2a. Experimental results for the mapping of S_1 (a'), S_2 (b'), and the polarization orientation ϕ (c') corresponding to pol-BIC$_1$. Numerical results of S_1 (a''), S_2 (b''), and polarization orientation (c''), as obtained from RCWA simulations of the active structure and corresponding to the pol-BIC$_1$.

experimental data. Both experimental and numerical results evidence clearly a polarization vortex, associated to a topological charge $q = -1$ of the LP branch at the Γ point. Most importantly, the striking similarity between the calculated polarization patterns of BIC$_1$ (Figures 4a,b,c) and the ones measured from pol-BIC$_1$ confirm that the topological charge of the purely photonic BIC, $q = -1$, has been fully transferred to the polaritonic one. In other words, the topological nature of pol-BICs is indeed originated from the purely photonic BIC components.

3 Conclusion

In conclusion, we have experimentally demonstrated the formation of polariton BICs at room temperature in a perovskite-based resonant metasurface. This is the first observation of the topological charge of polariton BICs. Moreover, the quasi-BIC nature, resulting from the hybridization between photonic BIC and excitonic resonance, is discussed and analyzed for the first time: as hybrid eigenmodes, these excitations

inherit the non-radiative losses from the excitonic component, but at the same time preserve the topological nature of the purely photonic BIC. Our results suggest that excitonic metasurface is a promising platform to reveal and exploit polariton effects (such as nonlinearity, or interaction with a magnetic field) with the engineering of polarization singularities. A straightforward application of the current work is to engineer polarization vortex beam lasing by reaching the Bose-Einstein condensation regime. Such highly directional coherent light sources, exhibiting polarization singularities at the center with doughnut-shape intensity, are highly desirable for applications in high-resolution imaging[57, 58]/focusing,[59, 60, 61] optical manipulation[62, 63]/communication,[64, 65] and data storage.[66] From a fundamental point of view, this would pave the way to explore new regimes of polariton condensation and quantum fluids of light, in which the condensate is totally decoupled from the radiative continuum and is purely non-radiative. Another attractive perspective is to use polariton nonlinearity, inherited from the excitonic component [36] to control the merging/splitting of topological charges,[5, 8] or to explore the multibistable regimes of BIC physics.[10, 12] Such a regime, only theoretically predicted,[10, 12] would pave the way towards ultrafast and low threshold all-optical devices such as polariton memories, switches, or transistors operating at room temperature.

4 Experimental and Theoretical section

Sample fabrication: The 2D structures were patterned using the laser interference lithography (LIL) technique. Substrates of 2 μm SiO_2/Si with size 1.5 x 1.5 cm were cleaned with acetone, ethanol, isopropanol then spincoated with photoresist MaN2403 at 5000 rpm in 30 sec then baked at 90°C in 1 min. These substrates were then put inside the LIL setup, exposed under laser λ=266 nm with power 8 mW. Following this, we developed the samples in AZ- MIF 726 solution in 20 s. After LIL process, the patterns were formed on photoresist film and later transferred on SiO_2 using reactive ion etching (RIE) method. SiO_2 was etched by a gas combination of CHF_3/SF_6/CH_4 with respectively 16:6.2:2 sccm at pressure 20 mTorr with power set to 60 W. Followed by the fabrication of 2D patterns, PEPI 10% in DMF was deposited on the patterns by spincoating at 3000 rpm in 30 sec then annealed at 95°C in 90 sec. Last, we encapsulated PEPI from oxygen and humidity by spin coating PMMA resist on top of the whole structure at 5000 rpm in 30 sec and baking at 95°C in 5 min.

Fourier spectroscopy: The sample is excited by a halogen lamp (for reflectivity and resonant scattering measurements) or by a non-resonant laser at 400 nm (for photoluminescence measurements) through a microscope objective (×20, NA=0.42). The scattered/emitter signal is collected via the same microscope objective and then is analyzed in the momentum space by imaging the backfocal plane of the microscope objective onto the camera sensor. For dispersion measurement, the signal is first projected onto the entrance a spectrometer whose output is coupled to the sensor of a CCD camera. For the farfield imaging, the signal is spectrally filtered by a band pass filter within 544 nm - 556 nm, and then projected onto the sensor of a SCMOS camera. Further information of the experimental setup is detailed in the Supporting Information.

Polarization mapping: The mapping of Stokes parameters, $S_1(k_x,k_y)$, $S_2(k_x,k_y)$ and $S_3(k_x,k_y)$, is directly extracted from the photoluminescence farfield images, which are analyzed in six different polarizations, respectively $\leftrightarrow$, $\updownarrow$, $\nearrow$, $\searrow$, $\circlearrowright$, $\circlearrowleft$. Then, the ellipticity, χ, is extracted from S_3: $\sin\{2\chi\} = S_3$; the orientation, ϕ, is extracted from S_1 and S_2 as $\tan\{2\phi\} = S_2/S_1$.

GME calculations and theory of light-matter coupling: The GME calculations have been performed by assuming an asymmetric planar waveguide with air (silica) as top (bottom) cladding, a core made of 200 nm thick PMMA (refractive index 1.49), 30 nm of unpatterned PEPI layer (index 2.41), and a square photonic lattice of 150 nm-thick circular PEPI pillars in a silica (index 1.48) backbone, lattice constant 330 nm, and pillar radius $r/a = 0.2$. The Stokes parameters are then calculated from the corresponding Bloch modes as[20] $c_x(k_x,k_y) = \hat{x}\cdot\langle u(k_x,k_y)\rangle$ and $c_y(k_x,k_y) = \hat{y}\cdot\langle u(k_x,k_y)\rangle$, where the Bloch functions u are calculated within the metasurface core (specifically, at half thickness of the patterned silica backbone), and the average $\langle u\rangle$ is performed on the direct lattice unit cell. From these, we calculate $S_1 = |c_x|^2 - |c_y|^2$, $S_2 = 2\,\mathrm{Re}\{c_x^* c_y\}$, and $S_3 = 2\,\mathrm{Im}\{c_x^* c_y\}$. Finally, the Stokes parameters are normalized as $(S_1^2 + S_2^2 + S_3^2)^{1/2} = 1$.

We notice that the Rabi coupling in polaritonic systems with confined excitons can be expressed in terms of the bulk value as

$$\hbar\omega_c \simeq \frac{\hbar\Omega}{2} = \hbar\omega_{\mathrm{bulk}}\sqrt{\frac{L_w}{L_{\mathrm{eff}}}} \tag{3}$$

in which $\hbar\omega_{\mathrm{bulk}} = \sqrt{A_X}/n$, L_w is the thickness of the active layer (i.e., where the field is mostly intense), A_X is the exciton oscillator strength of the active medium (expressed in eV^2, see next section), and L_{eff} is the effective confinement length of the evanescently decaying electric field. The latter quantities can be estimated from the field profile in Figure 2b, i.e., $L_w \sim 30$ nm, $L_{\mathrm{eff}} \sim 300$ nm. With these estimates we get $\hbar\Omega \simeq 240$ meV, in good agreement with the experimentally determined value.

RCWA simulations: The RCWA simulations have been performed with the S^4 package provided by the Fan Group at the Stanford Electrical Engineering Department.[67] The dielectric function of PEPI, used in RCWA simulations, is given by:

$$\varepsilon_{PEPI}(E) = n^2 + \frac{A_X}{E_X^2 - E^2 - i\gamma_X E} \tag{4}$$

where $n = 2.4$ is the refractive index of the passive structure, $A_X = 0.85\,\mathrm{eV}^2$ is the oscillator strength of PEPI exciton, $E_X = 2.394\,\mathrm{eV}$ is its energy and $\gamma_X = 30\,\mathrm{meV}$ is its linewidth.[38]

Supporting Information

Supporting Information is available from the Wiley Online Library or from the author.

Acknowledgements

The authors would like to thank the staff from the Nanolyon Technical Platform for helping and supporting in all nanofabrication processes. This work is partly supported by the French National Research Agency (ANR) under the project POPEYE (ANR-17-CE24-0020), project EMIPERO (ANR-18-CE24-

0016) and the IDEXLYON from Université de Lyon, Scientific Breakthrough project TORE within the Programme Investissements d'Avenir (ANR-19-IDEX-0005). DS and DG acknowledge financial support from the Italian Ministry of Research (MIUR) through the PRIN 2017 project "Interacting photons in polariton circuits" (INPhoPOL).

References

[1] J. Von Neumann, E. Wigner, *Z. Phys* **1929**, *30* 465.

[2] C. W. Hsu, B. Zhen, A. D. Stone, J. D. Joannopoulos, M. Soljačić, *Nature Reviews Materials* **2016**, *1*, 18 16048.

[3] S. I. Azzam, A. V. Kildishev, *Advanced Optical Materials* **2021**, *9*, 1 2001469.

[4] A. Kodigala, T. Lepetit, Q. Gu, B. Bahari, Y. Fainman, B. Kanté, *Nature* **2017**, *541*, 7636 196.

[5] J. Jin, X. Yin, L. Ni, M. Soljačić, B. Zhen, C. Peng, *Nature* **2019**, *574*, 7779 501.

[6] M. Wu, S. T. Ha, S. Shendre, E. G. Durmusoglu, W.-K. Koh, D. R. Abujetas, J. A. Sánchez-Gil, R. Paniagua-Domínguez, H. V. Demir, A. I. Kuznetsov, *Nano Letters* **2020**, *20*, 8 6005.

[7] C. Huang, C. Zhang, S. Xiao, Y. Wang, Y. Fan, Y. Liu, N. Zhang, G. Qu, H. Ji, J. Han, L. Ge, Y. Kivshar, Q. Song, *Science* **2020**, *367*, 6481 1018.

[8] M.-S. Hwang, H.-C. Lee, K.-H. Kim, K.-Y. Jeong, S.-H. Kwon, K. Koshelev, Y. Kivshar, H.-G. Park, *Nature Communications* **2021**, *12*, 1 4135.

[9] S. Romano, G. Zito, S. Torino, G. Calafiore, E. Penzo, G. Coppola, S. Cabrini, I. Rendina, V. Mocella, *Photon. Res.* **2018**, *6*, 7 726.

[10] S. D. Krasikov, A. A. Bogdanov, I. V. Iorsh, *Phys. Rev. B* **2018**, *97* 224309.

[11] M. Minkov, D. Gerace, S. Fan, *Optica* **2019**, *6*, 8 1039.

[12] V. A. Zakharov, A. N. Poddubny, *Phys. Rev. A* **2020**, *101* 043848.

[13] J. Wang, M. Clementi, M. Minkov, A. Barone, J.-F. Carlin, N. Grandjean, D. Gerace, S. Fan, M. Galli, R. Houdré, *Optica* **2020**, *7*, 9 1126.

[14] B. Zhen, C. W. Hsu, L. Lu, A. D. Stone, M. Soljačić, *Physical Review Letters* **2014**, *113*, 25 1.

[15] H. M. Doeleman, F. Monticone, W. den Hollander, A. Alù, A. F. Koenderink, *Nature Photonics* **2018**, *12*, 7 397.

[16] Y. Zhang, A. Chen, W. Liu, C. W. Hsu, B. Wang, F. Guan, X. Liu, L. Shi, L. Lu, J. Zi, *Phys. Rev. Lett.* **2018**, *120* 186103.

[17] B. Wang, W. Liu, M. Zhao, J. Wang, Y. Zhang, A. Chen, F. Guan, X. Liu, L. Shi, J. Zi, *Nature Photonics* **2020**, *14*, 10 623.

[18] X. Yin, J. Jin, M. Soljačić, C. Peng, B. Zhen, Observation of unidirectional bound states in the continuum enabled by topological defects, **2019**.

[19] W. Ye, Y. Gao, J. Liu, *Phys. Rev. Lett.* **2020**, *124* 153904.

[20] T. Yoda, M. Notomi, *Phys. Rev. Lett.* **2020**, *125* 053902.

[21] C. Weisbuch, M. Nishioka, A. Ishikawa, Y. Arakawa, *Phys. Rev. Lett.* **1992**, *69* 3314.

[22] J. Kasprzak, M. Richard, S. Kundermann, A. Baas, P. Jeambrun, J. M. J. Keeling, F. M. Marchetti, M. H. Szymańska, R. André, J. L. Staehli, V. Savona, P. B. Littlewood, B. Deveaud, L. S. Dang, *Nature* **2006**, *443*, 7110 409.

[23] I. Carusotto, C. Ciuti, *Rev. Mod. Phys.* **2013**, *85* 299.

[24] S. Christopoulos, G. B. H. Von Högersthal, a. J. D. Grundy, P. G. Lagoudakis, a. V. Kavokin, J. J. Baumberg, G. Christmann, R. Butté, E. Feltin, J. F. Carlin, N. Grandjean, *Physical Review Letters* **2007**, *98*, 12 1.

[25] K. S. Daskalakis, P. S. Eldridge, G. Christmann, E. Trichas, R. Murray, E. Iliopoulos, E. Monroy, N. T. Pelekanos, J. J. Baumberg, P. G. Savvidis, *Applied Physics Letters* **2013**, *102*, 10.

[26] H. Franke, C. Sturm, R. Schmidt-Grund, G. Wagner, M. Grundmann, *New Journal of Physics* **2012**, *14*, 1 13037.

[27] D. G. Lidzey, D. D. C. Bradley, M. S. Skolnick, T. Virgili, S. Walker, D. M. Whittaker, *Nature* **1998**, *395*, 6697 53.

[28] J. D. Plumhof, T. Stöferle, L. Mai, U. Scherf, R. F. Mahrt, *Nature Materials* **2014**, *13*, 3 247.

[29] X. Liu, T. Galfsky, Z. Sun, F. Xia, E.-c. Lin, Y.-H. Lee, S. Kéna-Cohen, V. M. Menon, *Nature Photonics* **2014**, *9* 30.

[30] G. Grosso, *Nature Photonics* **2017**, *11*, 8 455.

[31] T. Fujita, Y. Sato, T. Kuitani, T. Ishihara, *Phys. Rev. B* **1998**, *57*, 19 12428.

[32] N. Takada, T. Kamata, D. D. C. Bradley, *Applied Physics Letters* **2003**, *82*, 12 1812.

[33] G. Lanty, A. Bréhier, R. Parashkov, J.-S. Lauret, E. Deleporte, *New Journal of Physics* **2008**, *10*, 6 65007.

[34] H. S. Nguyen, Z. Han, K. Abdel-Baki, X. Lafosse, A. Amo, J. S. Lauret, E. Deleporte, S. Bouchoule, J. Bloch, *Applied Physics Letters* **2014**, *104*, 8 1.

[35] R. Su, C. Diederichs, J. Wang, T. C. H. Liew, J. Zhao, S. Liu, W. Xu, Z. Chen, Q. Xiong, *Nano Letters* **2017**, *17*, 6 3982.

[36] A. Fieramosca, L. De Marco, M. Passoni, L. Polimeno, A. Rizzo, B. L. T. Rosa, G. Cruciani, L. Dominici, M. De Giorgi, G. Gigli, L. C. Andreani, D. Gerace, D. Ballarini, D. Sanvitto, *ACS Photonics* **2018**, *5*, 10 4179.

[37] R. Su, S. Ghosh, J. Wang, S. Liu, C. Diederichs, T. C. H. Liew, Q. Xiong, *Nature Physics* **2020**.

[38] N. H. M. Dang, D. Gerace, E. Drouard, G. Trippé-Allard, F. Lédée, R. Mazurczyk, E. Deleporte, C. Seassal, H. S. Nguyen, *Nano Letters* **2020**, *20*, 3 2113.

[39] R. Su, E. Estrecho, D. Biegańska, Y. Huang, M. Wurdack, M. Pieczarka, A. G. Truscott, T. C. H. Liew, E. A. Ostrovskaya, Q. Xiong, *Science Advances* **2021**, *7*, 45 eabj8905.

[40] S. Zhang, Q. Shang, W. Du, J. Shi, Z. Wu, Y. Mi, J. Chen, F. Liu, Y. Li, M. Liu, Q. Zhang, X. Liu, *Advanced Optical Materials* **2018**, *6*, 2 1701032.

[41] Q. Shang, M. Li, L. Zhao, D. Chen, S. Zhang, S. Chen, P. Gao, C. Shen, J. Xing, G. Xing, B. Shen, X. Liu, Q. Zhang, *Nano Letters* **2020**, *20*, 9 6636, pMID: 32786951.

[42] K. L. Koshelev, S. K. Sychev, Z. F. Sadrieva, A. A. Bogdanov, I. V. Iorsh, *Phys. Rev. B* **2018**, *98* 161113.

[43] L. Lu, Q. Le-Van, L. Ferrier, E. Drouard, C. Seassal, H. S. Nguyen, *Photon. Res.* **2020**, *8*, 12 A91.

[44] P. Xie, Z. Liang, T. Jia, D. Li, Y. Chen, P. Chang, H. Zhang, W. Wang, *Phys. Rev. B* **2021**, *104* 125446.

[45] I. A. M. Al-Ani, K. As'Ham, L. Huang, A. E. Miroshnichenko, W. Lei, H. T. Hattori, *Advanced Optical Materials* **2021**, *n/a*, n/a 2101120.

[46] V. Kravtsov, E. Khestanova, F. A. Benimetskiy, T. Ivanova, A. K. Samusev, I. S. Sinev, D. Pidgayko, A. M. Mozharov, I. S. Mukhin, M. S. Lozhkin, Y. V. Kapitonov, A. S. Brichkin, V. D. Kulakovskii, I. A. Shelykh, A. I. Tartakovskii, P. M. Walker, M. S. Skolnick, D. N. Krizhanovskii, I. V. Iorsh, *Light: Science & Applications* **2020**, *9*, 1 56.

[47] V. Ardizzone, F. Riminucci, S. Zanottiy, A. Gianfrate, D. G. Suarez-Forero, F. Todisco, M. D. Giorgi, D. Trypogeorgos, G. Gigli, H. S. Nguyen, K. Baldwin, L. Pfeiffer, D. Ballarini, D. Gerace, D. Sanvitto **2021**.

[48] R. Su, A. Fieramosca, Q. Zhang, H. S. Nguyen, E. Deleporte, Z. Chen, D. Sanvitto, T. C. H. Liew, Q. Xiong, *Nature Materials* **2021**, *20* 1315.

[49] J. Tian, G. Adamo, H. Liu, M. Wu, M. Klein, J. Deng, N. S. S. Ang, R. Paniagua-Domínguez, H. Liu, A. I. Kuznetsov, C. Soci, Phase-change perovskite tunable microlaser, **2021**.

[50] K. Gauthron, J.-S. Lauret, L. Doyennette, G. Lanty, A. A. Choueiry, S. J. Zhang, A. Brehier, L. Largeau, O. Mauguin, J. Bloch, E. Deleporte, *Opt. Express* **2010**, *18*, 6 5912.

[51] L. C. Andreani, D. Gerace, *Phys. Rev. B* **2006**, *73* 235114.

[52] M. Minkov, I. A. D. Williamson, L. C. Andreani, D. Gerace, B. Lou, A. Y. Song, T. W. Hughes, S. Fan, *ACS Photonics* **2020**, *7*, 7 1729.

[53] D. Gerace, L. C. Andreani, *Phys. Rev. B* **2007**, *75* 235325.

[54] A. Auffèves, D. Gerace, M. Richard, S. Portolan, M. França Santos, L. C. Kwek, C. Miniatura, *Strong Light-Matter Coupling*, WORLD SCIENTIFIC, **2014**.

[55] M. Galli, D. Bajoni, M. Belotti, F. Paleari, M. Patrini, G. Guizzetti, D. Gerace, M. Agio, L. Andreani, D. Peyrade, Y. Chen, *IEEE Journal on Selected Areas in Communications* **2005**, *23*, 7 1402.

[56] M. W. McCutcheon, G. W. Rieger, I. W. Cheung, J. F. Young, D. Dalacu, S. Frédérick, P. J. Poole, G. C. Aers, R. L. Williams, *Applied Physics Letters* **2005**, *87*, 22 221110.

[57] D. P. Biss, K. S. Youngworth, T. G. Brown, *Appl. Opt.* **2006**, *45*, 3 470.

[58] R. Chen, K. Agarwal, C. J. R. Sheppard, X. Chen, *Opt. Lett.* **2013**, *38*, 16 3111.

[59] K. S. Youngworth, T. G. Brown, *Opt. Express* **2000**, *7*, 2 77.

[60] R. Dorn, S. Quabis, G. Leuchs, *Phys. Rev. Lett.* **2003**, *91* 233901.

[61] T. Bauer, S. Orlov, U. Peschel, P. Banzer, G. Leuchs, *Nature Photonics* **2014**, *8*, 1 23.

[62] Y. Kozawa, S. Sato, *Opt. Express* **2010**, *18*, 10 10828.

[63] C. Min, Z. Shen, J. Shen, Y. Zhang, H. Fang, G. Yuan, L. Du, S. Zhu, T. Lei, X. Yuan, *Nature Communications* **2013**, *4*, 1 2891.

[64] Y. Zhao, J. Wang, *Opt. Lett.* **2015**, *40*, 21 4843.

[65] G. Milione, T. A. Nguyen, J. Leach, D. A. Nolan, R. R. Alfano, *Opt. Lett.* **2015**, *40*, 21 4887.

[66] F. Cardano, E. Karimi, S. Slussarenko, L. Marrucci, C. de Lisio, E. Santamato, *Appl. Opt.* **2012**, *51*, 10 C1.

[67] V. Liu, S. Fan, *Computer Physics Communications* **2012**, *183*, 10 2233.